THE JOURNAL OF BIOLOGICAL CHEMISTRY VOL. 288, NO. 50, pp. 35736–35748, December 13, 2013

The Orphan Adhesion G Protein-coupled Receptor GPR97 Regulates Migration of Lymphatic Endothelial Cells via the Small GTPases RhoA and Cdc42*

Received for publication, August 22, 2013, and in revised form, October 21, 2013 Published, JBC Papers in Press, October 31, 2013, DOI 10.1074/jbc.M113.512954

Nadejda Valtcheva, Adriana Primorac, Giorgia Jurisic[1], Maija Hollmén, and Michael Detmar[2]

From the Institute of Pharmaceutical Sciences, ETH Zurich, Wolfgang-Pauli-Strasse 10, 8093 Zurich, Switzerland

Background: The identification of G protein-coupled receptors (GPCRs) specific for the lymphatic endothelial cells (LECs) is essential for establishing drugs targeting the lymphatic system.
Results: GPR97 is an orphan adhesion GPCR that regulates LEC migration.
Conclusion: GPR97 is the first known adhesion GPCR involved in lymphatic remodeling.
Significance: This first evidence that adhesion GPCRs govern LEC motility opens new possibilities for modulating lymphangiogenesis.

The important role of the lymphatic vascular system in pathological conditions such as inflammation and cancer has been increasingly recognized, but its potential as a pharmacological target is poorly exploited. Our study aimed at the identification and molecular characterization of lymphatic-specific G protein-coupled receptors (GPCRs) to assess new targets for pharmacological manipulation of the lymphatic vascular system. We used a TaqMan quantitative RT-PCR-based low density array to determine the GPCR expression profiles of *ex vivo* isolated intestinal mouse lymphatic (LECs) and blood vascular endothelial cells (BECs). GPR97, an orphan adhesion GPCR of unknown function, was the most highly and specifically expressed GPCR in mouse lymphatic endothelium. Using siRNA silencing, we found that GPR97-deficient primary human LECs displayed increased adhesion and collective cell migration, whereas single cell migration was decreased as compared with nontargeting siRNA-transfected control LECs. Loss of GPR97 shifted the ratio of active Cdc42 and RhoA and initiated cytoskeletal rearrangements, including F-actin redistribution, paxillin and PAK4 phosphorylation, and β1-integrin activation. Our data suggest a possible role of GPR97 in lymphatic remodeling and furthermore provide the first insights into the biological functions of GPR97.

The lymphatic vascular system plays an important role in the drainage of interstitial protein-rich fluid, the transportation of immune cells to the lymph nodes, and the uptake of dietary fat from the intestine. The most prominent direct consequence of lymphatic vessel dysfunction is the enrichment of fluid in the tissue and the development of lymphedema. In recent years, it has become evident that the lymphatic vasculature and its expansion through a process termed lymphangiogenesis have a far more dramatic impact upon disease progression than previously thought (1–3). For instance, lymphatic vessels facilitate the dissemination of cancer cells not only through providing the "roads" to the draining lymph nodes and distant organs, but also by actively enhancing tumor spread via secretion of chemokines (4). In contrast, the activation of lymphatic vessels can limit acute and chronic skin inflammation, likely by increasing the drainage of tissue fluid and of inflammatory mediators and cells (5, 6). As compared with the increasing knowledge on the impact of lymphangiogenesis in human pathologies, the advances regarding new lymphatic-based treatment strategies are rather moderate. Only very recently, the first anti-lymphangiogenic treatment, an antibody against vascular endothelial growth factor (VEGF) receptor-3, entered clinical cancer trials (7). The lack of pharmacological modulators is partially due to the poor characterization of "druggable" proteins expressed specifically on the lymphatic vessels, a fact underscoring the need for the identification of new lymphatic markers suitable as drug targets. Regarding their potential as therapeutic targets, G protein-coupled receptors (GPCRs)[3] are among the most promising candidates. Indeed, 30% of the currently marketed pharmaceuticals target GPCRs covering a broad range of indications from hypertension to allergy (8). The GPCRs are heptahelical transmembrane receptors that sense a variety of chemical and physical signals and therefore play a role in the majority of biological processes. The importance of the GPCRs is underpinned by the huge number of genes encoding for more than 1000 different receptors found in the human genome. Only a few GPCRs, for instance the adrenomedullin receptor, have been found to be enriched in the lymphatic endothelium and to be crucial for lymphangiogenesis (9). The paucity of known lymphatic-specific GPCRs is at least partly due to difficulties generally encountered in the GPCR research

* This work was supported by Swiss National Science Foundation Grant 31003A-130627, European Research Council Grant LYVICAM, Oncosuisse, Krebsliga Zurich, and the Leducq Foundation.

[1] Present address: Novartis Institutes for BioMedical Research, Novartis Pharma AG, CH-4056 Basel, Switzerland.

[2] To whom correspondence should be addressed: Institute of Pharmaceutical Sciences, Swiss Federal Institute of Technology, ETH Zurich, Wolfgang Pauli Str. 10, HCI H303, CH-8093 Zurich, Switzerland. Tel.: 41-44-633-7361; Fax: 41-44-633-1364; E-mail: michael.detmar@pharma.ethz.ch.

[3] The abbreviations used are: GPCR, G protein-coupled receptor; 7TM, seven-transmembrane; BEC, blood vascular endothelial cell; LEC, lymphatic endothelial cell; MLC, myosin light chain; EBM, endothelial basal medium; qRT-PCR, quantitative RT-PCR; p, phospho.

field. The usually low number of receptors expressed on the cell membrane and the lack of specific antibodies are two major obstacles hampering the identification of new GPCRs at the protein level. Therefore, we thought that a genome-wide comparative transcriptional analysis of lymphatic endothelial cells (LECs) and the closely related blood vascular endothelial cells (BECs) might represent a more promising approach in the search of lymphatic-specific GPCRs. Several crucial and specific players in lymphatic biology have been identified with this approach using cultured endothelial cells (10–12). Because cultured cells lack important cues derived from the *in vivo* microenvironment, we have recently established a method for the *ex vivo* isolation of LECs and BECs directly from the mouse intestine followed by microarray analysis (13). These studies have identified novel mediators of lymphatic development, maturation, and function (13, 14). They also indicated that several GPCRs, including members of the recently described subclass of adhesion GPCRs, which combine adhesion and signaling features (15), might be differentially expressed in LECs *versus* BECs. This otherwise highly heterogenic GPCR subfamily shares an extended N-terminal domain, often comprising domains characteristic for adhesion molecules linked to the 7TM stretches by a GPCR proteolytic site (16, 17). The vast majority of adhesion GPCRs are still orphan receptors, and evidence that they exhibit classical signaling has only recently been provided (18, 19). In contrast to fairly well characterized adhesion GPCRs such as the EGF-7TM receptors (20), the only hint for the function of others is their tissue distribution reflected by microarray and expressed sequence tag data.

Several GPCRs are involved in the regulation of cell adhesion and migration (21). Because lymphangiogenesis, the growth of new lymphatic vessels from pre-existing ones, includes adhesion, migration, and extracellular matrix reorganization steps (22), we aimed to identify GPCRs specifically expressed in LECs (with a focus on the adhesion GPCRs) that might play a role in lymphangiogenic remodeling. Therefore, we performed a TaqMan qRT-PCR-based GPCR expression profiling in *ex vivo* isolated LECs and BECs from the mouse intestine. We identified the adhesion GPCR GPR97 (also known as Pb99) as the most LEC-specific GPCR and characterized its functions in LEC migration and adhesion.

EXPERIMENTAL PROCEDURES

RNA Isolation, Reverse Transcription, and TaqMan GPCR Array— 8-week-old C57BL/6J mice were sacrificed to obtain colon tissue for the *ex vivo* cell isolation of endothelial cells as described previously (13). RNA was directly isolated from the LEC and BEC populations, amplified, and reverse-transcribed. Resulting cDNAs (400 ng per sample per microfluidic card) were mixed with TaqMan universal PCR master mix (Applied Biosystems) and loaded in the mouse GPCR TaqMan low density array microfluidic cards (4378703, Applied Biosystems). qRT-PCR was carried out in the 7900HT fast real-time PCR system (Applied Biosystems) under the conditions recommended by the manufacturer. Data were analyzed according to the $2^{-\Delta\Delta}{}_{CT}$ method (23). Four animal-matched pairs of LEC and BEC were used.

Cell Culture—Human dermal LECs were isolated from neonatal human foreskins by immunomagnetic purification as described previously (11) or purchased from Promocell, Heidelberg, Germany. LECs were maintained as monolayers for up to nine passages as described elsewhere (11).

Transient siRNA Knockdown and GPR97 Overexpression—LECs between passage 7 and 9 were transfected with either scrambled control (Silencer Negative Control No. 1, catalog number AM4611, Ambion; Life Technologies) siRNA or two GPR97-targeting siRNAs referred to as 97 si1 and 97 si2 (ID: s48198 and s48199, catalog number 4392420 Ambion, Life Technologies) alone or together with pcDNA5FRT_CAT (pCAT: control vector expressing chloramphenicol-transferase) or pcDNA5FRT_HA-N97 (pHA-N97: GPR97 tagged N-terminally with HA tag) using the basic Nucleofector kit for primary mammalian endothelial cells and the Amaxa Nucleofector II electroporator according to the manufacturer's instructions (Lonza). $4-8 \times 10^5$ cells were electroporated with 50 pmol (when s48198 and s4819 were combined, 25 pmol of each were used).

SYBR Real-time Quantitative PCR and Western Blot—2×10^5, 1.5×10^5, or 10^5 LECs were seeded into 6-well plates after siRNA electroporation and harvested with 1 ml/well TRIzol (Life Technologies) after 24, 48, and 72 h, respectively. RNA and protein were isolated according to the manufacturer's protocol. RNA was purified with the RNeasy kit (Qiagen) according to the manufacturer's instructions. Proteins were isolated from the remaining organic phase and resuspended in 1% SDS, 100 mM Tris-HCl, pH 8.0. Protein concentration was determined with the Pierce BCA protein assay kit (Thermo Fischer Scientific).

Total RNA was transcribed to cDNA with the high capacity cDNA reverse transcription kit (Life Technologies). qRT-PCR was performed in triplicates with SYBR kit (Roche Applied Science) and the QuantiTect primer assay (Qiagen; 204143; Hs_GPR97_1_SG QuantiTect primer assay QT00065653). 50 ng of cDNA per 20-μl reaction were used. Human β-actin was used as an internal control (forward primer 5′-TCACCGAGCGCGGCT-3′; reverse primer 5′-TAATGTCACGCACGATTTCCC-3′; Sigma-Aldrich). The relative expression of GPR97 (normalized to β-actin) was expressed as the percentage of the relative expression in the scrambled-transfected LECs.

Equal amounts of the protein samples were incubated for 10 min at 70 °C in Laemmli buffer (0.05 M Tris-HCl pH 6.8; 10% glycerol, 2% SDS, 0.1 M DTT, 0.005% bromphenol blue), resolved with 10% polyacrylamide gels or precasted NuPage (Life Technologies), and transferred to Immobilon P PVDF membranes (Millipore Biosciences). Membranes were blocked for 1 h at room temperature in 5% nonfat dry milk in TBS-T and incubated overnight at 4 °C with primary antibodies in 1% nonfat dry milk in TBS-T against human GPR97 (rabbit, Abcam, Cambridge, UK; Ab122653, 1:300), GAPDH (rabbit, Sigma-Aldrich; G9545, 1:1000), MAPK (Cell Signaling, 9102, 1:2000); all others 1:500 p-MAPK (Cell Signaling, 9212), p-Src (Cell Signaling, 2191), p-PKCpan (Cell Signaling, 9371), p-MLC (Abcam, ab2480), p-AKT (Cell Signaling, 9271), β-actin (Abcam, 8229), Cdc42 (Cytoskeleton, ACD03), p-cofilin (Cell Signaling, 3313),

p-PAK4/5/6 (Cell Signaling, 3241), and p-PaxillinY31 (Sigma-Aldrich, 6368).

Wound Healing (Scratch) Assay—7×10^4 LECs/well were cultured in EBM full medium for 24 h after siRNA electroporation or 36 h after siRNA and plasmid DNA electroporation in 24-well plates coated with 10 μg/ml fibronectin or 50 μg/ml type I collagen. Cells were starved for 4 h (EBM, L-glutamine, antibiotics, 2% FBS) before two cross-shaped scratches were introduced to the confluent monolayer with a sterile pipette tip. After PBS washing, starvation medium was replaced by full EBM with or without the supplements to be tested. Pictures of the two cross points per well were taken at time points $t = 0$ and $t = 17$ h at a 5× magnification (A-plan objective 5×/0.12, Zeiss Axiovert 200M microscope, Zeiss AxioCam MRm camera, Carl Zeiss Microscopy, Jena, Germany), and the percentage of the open area was analyzed automatically with the TScratch software (24). Cells were incubated with 20 ng/ml recombinant VEGF-A (R&D Systems, Minneapolis, MN) and treated with 0.5 units/ml CN03 (Cytoskeleton, Denver, CO) or 1 unit/ml CN02 (Cytoskeleton) for 4 h and then incubated in full EBM medium. Conditioned media were collected from either scrambled control or GPR97-targeting siRNA-treated cells at a time point corresponding to the $t = 17$ h of the wound healing assay. After removing the cell debris (centrifugation for 5 min at room temperature and $300 \times g$), the supernatants were mixed at a 1:2 ratio with full EBM and were added to the cells at $t = 0$ h of the scratch assay until the end time point.

Adhesion and Transwell Migration Assays—LECs (10^6) were plated after siRNA electroporation on fibronectin-coated 100-mm dishes and were cultured for 24 h in full EBM medium. After 4 h of starvation (EBM with 2% FBS), adhesion and Transwell migration assays were performed.

For adhesion assays, 96-well plates (Costar black clear bottom, Corning Inc., Corning, NY) were coated with 10 μg/ml fibronectin or 50 μg/ml type I collagen followed by 1 h of blocking with 0.2% BSA in PBS. Scrambled and GPR97 siRNA-transfected LECs were labeled in suspension for 15 min at 37 °C with 4 μg/ml calcein AM (Life Technologies) in PBS. After washing with 0.2% BSA in PBS, 4×10^4 cells were plated per well. Cells were allowed to adhere at 37 °C for 45 min, and unattached cells were removed by three gentle washes with 0.2% BSA in PBS. Fluorescence ($\lambda_{ex} = 485$ nm $\lambda_{em} = 538$ nm) was measured in a microplate reader (Spectra Max Gemini EM, Molecular Devices).

To measure chemotaxis, haptotaxis, or single cell motility, different variations of the Transwell migration assay were used. 24-well Transwell inserts of 8-μm pore size (Corning Inc.) were coated for 1 h with 10 μg/ml fibronectin on the bottom side for haptotaxis or on both sides for chemotaxis and single cell motility and were subsequently blocked with 2% BSA in PBS. 5×10^4 of scrambled or GPR97 siRNA-transfected LECs in 0.5% BSA containing basal EBM were plated onto the inserts. For the chemotaxis assays, EBM containing 3% FBS was added to the lower well. For the haptotaxis and single cell motility assays, the same medium was added to the upper and lower wells (EBM containing 0.5% BSA). Cells were allowed to transmigrate at 37 h for 3.5 h before the inserts were vigorously washed with PBS, and the cells on the top side were removed with a cotton swab. Transmigrated cells were methanol-fixed and stained with 1:5000 Hoechst 33342 (Life Technologies), and the porous membranes were excised from the inserts and mounted on glass slides. Samples were analyzed with the Axioskop 2 mot plus upright microscope using A-plan objective 5×/0.12, and images were taken with Zeiss AxioCam MRm camera.

RhoA-GTP and Cdc42-GTP Determination with G-LISA—Scrambled and GPR97 siRNA-transfected LECs were cultured for 24 h after electroporation on fibronectin-coated 6-well plates (2×10^5 cells/well) in full EBM medium and were subsequently starved overnight. For Cdc42 or RhoA activation, cells were incubated in basal EBM containing or not containing 2 units/ml of the Cdc42 activator CN02 (Cytoskeleton) or 1 unit/ml of the RhoA activator CN03 (Cytoskeleton) for 2 or 30 min, respectively. LECs were washed in PBS twice on ice and were rapidly lysed with the corresponding lysis buffer included in the G-LISA kits (BK124 for RhoA and BK127 for Cdc42). Cell lysates were snap-frozen in liquid nitrogen and stored at −80 °C until they were processed according to manufacturer's manual. Total RhoA was determined by ELISA (Cytoskeleton, BK150).

Flow Cytometry, Immunofluorescence Stains, and Confocal Microscopy—After siRNA electroporation, LECs were cultured for 24 h on fibronectin-coated 100-mm dishes (10^6 cells) or on two-chamber Lab-Tek glass slides (Thermo Fischer Scientific, Roskilde, Denmark; 4×10^5 cells/chamber) in full EBM medium. Subsequently, cells were starved overnight in EBM containing 2% FBS.

For flow cytometry analyses, LECs were detached with Accutase and washed in PBS. 10^5 cells were fixed and stained with either 9EG7 rat anti-mouse active β1-integrin antibody (BD Biosciences; 553715; 1:150 diluted in 2% FBS in PBS-Ca^{2+}/Mg^{2+}) or anti-human total β1-integrin antibody (Millipore; MAB-2247-I; 1:150 diluted in 2% FBS in PBS-Ca^{2+}/Mg^{2+}) IgG_{2a} control followed by allophycocyanin-coupled goat anti-rat IgG (Life Technologies; R40005; 1:200). 10^4 events per sample were recorded with a FACSCanto, and data were analyzed with FlowJo software.

For immunofluorescence stains of active β1-integrin, LECs were fixed with 4% formaldehyde in PBS on two-chamber Lab-Tek glass slides, and active β1-integrin was stained for 30 min at room temperature with rat anti-mouse antibody 9EG7 against the active β1-integrin (BD Biosciences; 553715; 1:100) in PBS-Ca^{2+}/Mg^{2+} visualized with Alexa Fluor 488-coupled donkey anti-rat antibody (Life Technologies, A21208, 1:400). Nuclei were stained with Hoechst 33342 (Life Technologies, A21202, 1:5000). The cytoskeletal stains were performed on two-chamber Lab-Tek glass slides with the F-actin Visualization Biochem kit (Cytoskeleton, BK005) followed by immunostaining of vinculin (Sigma-Aldrich, V9131, 1:400).

Confocal microscopy was performed with a Leica SP2-FCS DMIRE2 (inverse) system, using a $63 \times 1.4-0.6$NA differential interference contrast, oil immersion, HCX Plan-Apo (blue-corrected) objective. Images were taken using the Leica LCS Software. Maximum intensity projection of the Z-stacks were analyzed with ImageJ.

TABLE 1

GPCRs and modulators of GPCR signaling differentially expressed in *ex vivo* isolated mouse LECs; listed below are genes expressed more strongly in LECs

qRT-PCR-based low density array analysis revealed differences in the GPCR expression pattern in *ex vivo* isolated mouse intestinal LECs. Selected genes with significantly changed expression are shown. Members of the adhesion GPCR family are bolded.

Gene		-Fold LEC/BEC	*p*
Gpr97[a]	**G protein-coupled receptor 97**	14,4050.5	5.46×10^{-6}
Gprc5c	G protein-coupled receptor, family C, group 5, member C	1390.5	3.23×10^{-3}
Gpr77[a]	G protein-coupled receptor 77	729.1	1.82×10^{-3}
F2rl1	Coagulation factor II (thrombin) receptor-like 1	304.7	2.93×10^{-2}
Frzb[a]	Frizzled-related protein	214.4	2.01×10^{-3}
Gpr124	**G protein-coupled receptor 124**	203.3	1.21×10^{-2}
Celsr1[a]	**Cadherin EGF LAG seven-pass G type receptor 1**	166.8	4.20×10^{-5}
Tm7sf3	Transmembrane 7 superfamily member 3	18.7	7.24×10^{-3}
F2r	Coagulation factor II (thrombin) receptor	12.6	3.39×10^{-2}
Admr	Adrenomedullin receptor	6.3	3.26×10^{-3}
Adora2a	Adenosine A2a receptor	3.5	5.75×10^{-2}
Adrb2	Adrenergic receptor, β 2	2.8	4.22×10^{-2}

[a] C_T values in BECs > 36.

TABLE 2

GPCRs and modulators of GPCR signaling differentially expressed in *ex vivo* isolated mouse BECs; listed below are genes expressed more strongly in BECs

qRT-PCR-based Low Density Array analysis revealed differences in the GPCR expression pattern in *ex vivo* isolated mouse intestinal BECs. Selected genes with significantly changed expression are shown. Members of the adhesion GPCR family are bolded.

Gene		-Fold BEC/LEC	*p*
Cysltr1[a]	Cysteinyl leukotriene receptor 1	20,000.0	1.09×10^{-4}
Agtrl1[a]	Angiotensin receptor-like 1	15,275.4	1.63×10^{-4}
Ramp3	Receptor (calcitonin) activity-modifying protein 3	6004.1	1.70×10^{-4}
P2ry6[a]	Pyrimidinergic receptor P2Y, G protein-coupled, 6	4337.1	2.12×10^{-3}
Chrm2[a]	Cholinergic receptor, muscarinic 2, cardiac	1934.4	1.38×10^{-5}
Edg6[a]	Endothelial differentiation sphingolipid G protein-coupled receptor 6	986.8	5.60×10^{-3}
Cysltr2	Cysteinyl leukotriene receptor 2	888.7	6.06×10^{-5}
P2ry2[a]	Pyrimidinergic receptor P2Y, G protein-coupled, 2	581.9	9.11×10^{-4}
Gpr81[a]	G protein-coupled receptor 81	309.0	9.10×10^{-5}
Gpr17[a]	G protein-coupled receptor 17	264.5	9.27×10^{-5}
Lphn2	Latrophilin 2	171.1	1.84×10^{-2}
Gpr21	G protein-coupled receptor 21	162.7	4.13×10^{-2}
Gpr23	G protein-coupled receptor 23	119.1	6.06×10^{-3}
Gpr1	G protein-coupled receptor 1	97.9	3.07×10^{-2}
Gpr56	**G protein-coupled receptor 56**	42.5	3.62×10^{-4}
Lgr5	Leucine-rich repeat containing G protein-coupled receptor 5	34.7	2.78×10^{-2}
P2ry5	Pyrimidinergic receptor P2Y, G protein-coupled, 5	26.2	1.54×10^{-2}
Gpr160	G protein-coupled receptor 160	14.2	4.46×10^{-2}
Eltd1	EGF, latrophilin seven transmembrane domain containing 1	11.7	2.86×10^{-2}
Ccrl2	Chemokine (C-C motif) receptor-like 2	10.9	5.40×10^{-3}
Cd97	CD 97 antigen	3.8	1.73×10^{-2}

[a] C_T values in LECs > 36.

Statistical Analyses—Data were analyzed with GraphPad Prism applying the two-tailed unpaired *t* test with $p < 0.05$ considered significant.

RESULTS

GPCRs Are Differentially Expressed in ex Vivo Isolated Mouse LECs versus BECs—To identify GPCRs specifically expressed by murine LECs *in vivo*, we employed a method for RNA isolation from freshly sorted LECs and BECs from mouse intestines (13). Total RNA derived from four animal-matched pairs of *ex vivo* isolated mouse LECs and BECs was subjected to a whole transcriptome amplification and reverse transcription. The resulting cDNA was used in a qRT-PCR TaqMan low density array designed for the screening of proteins involved in GPCR signaling. The obtained results represent a comparative transcriptome analysis of GPCRs and modulators of GPCR signaling in LECs and BECs (Tables 1 and 2). Among the GPCRs that were differentially expressed in LECs *versus* BECs, several members of the new subclass of adhesion GPCRs were identified (Tables 1 and 2). GPR97, a member of this protein family, displayed the most striking difference with expression levels just above the detection threshold in BECs and with abundant expression in LECs (more than 100,000-fold higher expression, Tables 1 and 2). Also, two other adhesion GPCRs, namely GPR124 and Celsr1, were more strongly expressed by LECs *versus* BECs (203.3- and 166.8-fold up-regulation, respectively; Tables 1 and 2). GPR97 was also expressed in cultured primary human dermal LECs, as evaluated at the mRNA level by quantitative SYBR qRT-PCR (data not shown) and at the protein level by Western blotting (Fig. 1*B*, *ctr si*).

Silencing of GPR97 Enhances Collective Cell Migration of LECs—To explore the potential function of GPR97 in lymphatic biology, we silenced GPR97 in primary human LECs. We transfected LECs with either scrambled control or a pool of GPR97-targeting siRNAs and analyzed the knockdown efficiency over time because 7TM proteins have multiple levels of posttranslational control and can vary in their protein turnover kinetics. GPR97 RNA levels decreased in average to 13% of control levels at 24 h after transfection and recovered to approximately 50% of control after 72 h (Fig. 1*A*). Western blot analysis revealed a moderate reduction of GPR97 protein at 24 h and a strong decrease at 48 h after transfection, whereas no major

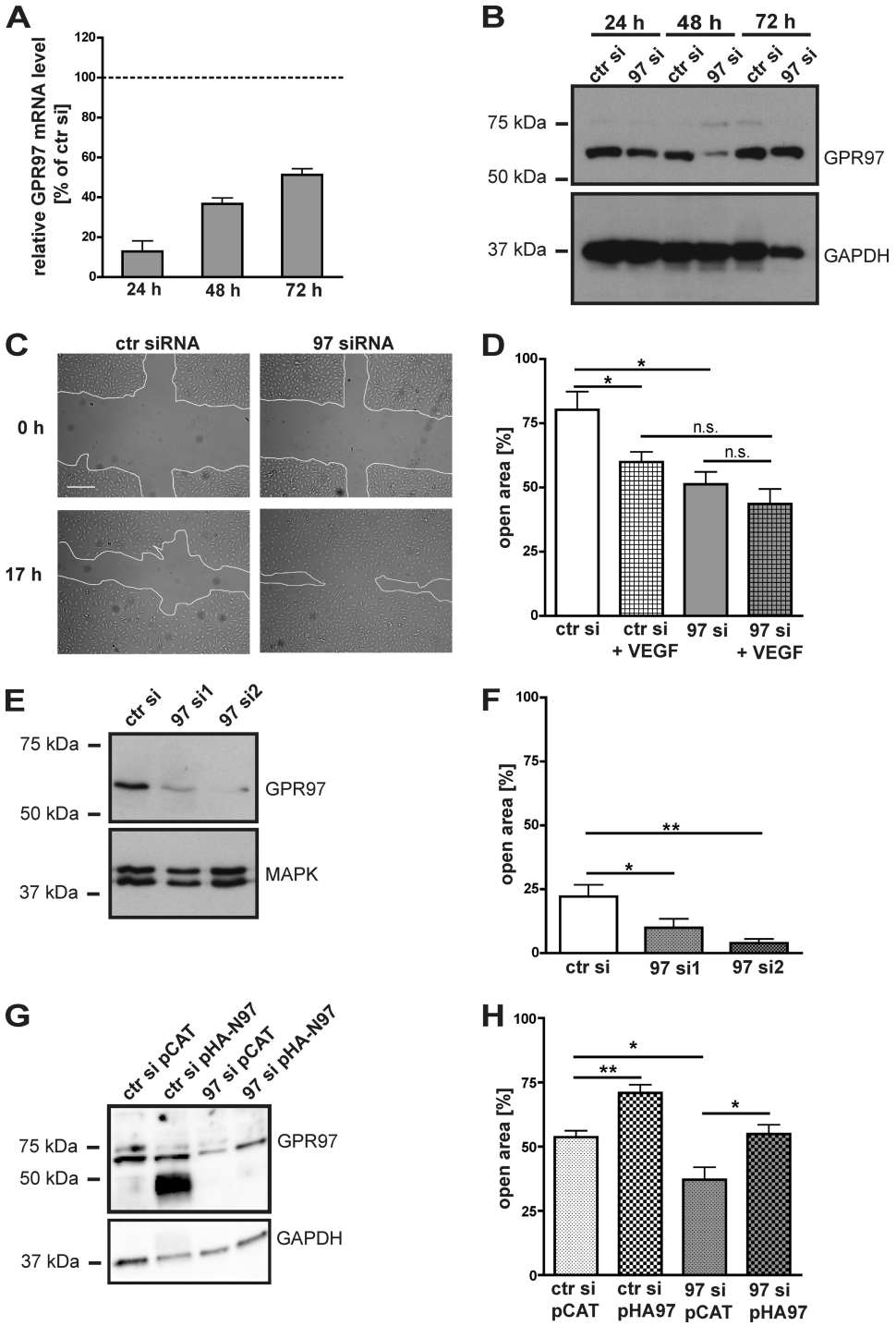

FIGURE 1. **GPR97 knockdown enhances collective cell migration of LECs.** *A* and *B*, knockdown efficiency obtained with a pool of GPR97-targeting siRNA (*97 si*) as compared with scrambled control siRNA (*ctr si*). GPR97 mRNA (*A*) and protein (*B*) levels were determined at different time points after transfection. GPR97 mRNA levels detected by SYBR qRT-PCR were normalized to β-actin mRNA. The bars represent mean $\pm$ S.E. from three experiments as the percentage of the values for the control siRNA (designated by the *dotted line*). GPR97 protein (61 kDa) was detected by Western blotting; GAPDH (36 kDa) was used as loading control. Representative image from three different experiments is shown. *C*, representative images from wound healing (scratch) assay at time points $t = 0$ and $t = 17$ h after wounding of the confluent cell layer show enhanced wound closure by the GPR97-deficient LECs. *D*, quantification of the wounded area (in %) that remained open at $t = 17$ h in scrambled control *versus* GPR97-deficient LEC monolayer was performed by the TScratch software tool. 20 ng/ml VEGF-A was applied as a migration-inducing stimulus. Mean $\pm$ S.E. $n = 4$ wells per condition (average of two scratches per well) is shown. *, $p < 0.05$. *E*, knockdown with two different GPR97-targeting siRNAs (*97 si1* and *97 si2*) leads to GPR97 loss as detected by Western blotting; MAPK (42/44 kDa) was used as loading control. *F*, quantification of the wounded area (in %) that remained open at $t = 17$ h in LEC monolayer was performed by the TScratch software tool. Both different GPR97-targeting siRNAs show increased wound closure as compared with the nontargeting scramble control. *G*, GPR97 expression after GPR97 knockdown in LECs. GPR97 protein levels were determined at time point 48 h after transfection. GPR97 protein (61 kDa, * cleaved C-terminal GPR97 32 kDa) was detected by Western blotting; GAPDH (37 kDa) was used as loading control. *pCAT*, control vector; *pHA-N97*, vector expressing HA-tagged full-length GPR97. *H*, expression of GPR97 reversed the enhanced collective cell migration of the GPR97-deficient cells and decreased the migration of the control siRNA transfected. Quantification of the wounded area (in %) that remained open at $t = 17$ h in LEC monolayer was determined by the TScratch software tool. *, $p < 0.05$, **, $p < 0.01$.

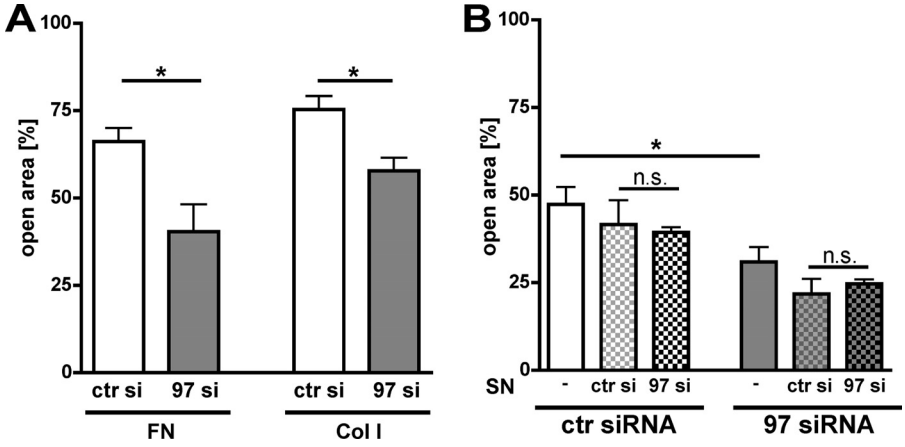

FIGURE 2. **The enhanced collective cell migration of GPR97-deficient LECs is not dependent on matrix components or secreted molecules.** *A* and *B*, quantification of the wound area (in %) of scrambled control *versus* GPR97-deficient LECs that remained open at $t = 17$ h by TScratch software tool, when cells were cultured on 10 μg/ml fibronectin (*FN*) *versus* 50 μg/ml type I collagen (*Col I*) (*A*) and in the presence of conditioned medium (*SN*) collected from scrambled control siRNA (*ctr si*)-transfected LECs (control siRNA supernatant) *versus* GPR97-targeting siRNA (*97 si*)-transfected LECs (GPR97 siRNA supernatant) (*B*). Mean ± S.E., $n = 4$ wells per condition (average of two scratches per well) is shown. *, $p < 0.05$.

reduction was found after 72 h (Fig. 1*B*). Thus, functional assays were carried out between 24 and 48 h after transfection. We first determined the collective cell migration of GPR97-deficient cells in a monolayer wound healing (scratch) assay. GPR97-deficient LECs closed the wounded area significantly faster than the scrambled control cells ($p = 0.015$, Fig. 1, *C* and *D*). This effect was of the same magnitude as the acceleration of wound closure seen after incubation with 20 ng/ml VEGF-A. GPR97 knockdown also slightly accelerated wound closure in the presence of VEGF-A. To exclude nontargeting effects, we performed the experiment with the two different siRNAs separately and could observe increased collective LEC migration in both cases (Fig. 1, *E* and *F*). Moreover, the magnitude of the effect correlated with the efficiency of the knockdown being stronger with siRNA2. The different migration potential under control conditions between Fig. 1, *D* and *F*, was due to the different migration potential of the different human LEC isolates used. Additionally, the effect of GPR97 silencing was reversed by the simultaneous transfection with a GPR97-encoding plasmid (Fig. 1, *G* and *H*). In the sample, in which GPR97 was overexpressed (GPR97-encoding plasmid co-transfected with the control siRNA), the majority of the protein was cleaved at the GPCR proteolytic site (Fig. 1*G*, *lower band*, *).

The Increased Collective Migration Capacity of GPR97-deficient Cells Is Not Dependent on the Coating Substrate or on Molecules Secreted after GPR97 Knockdown—Because some adhesion GPCRs exert their effects through direct binding to other adhesion molecules (25, 26), we next investigated whether the increased wound closure of GPR97-deficient LECs was due to loss of potential inhibitory interplay of GPR97 with matrix proteins. Thus, we next compared the effects of GPR97 knockdown on cell migration on fibronectin- *versus* collagen type I-coated wells. The increase in wound closure of the GPR97-deficient LECs, as compared with control cells, was similar on both coating substrates (Fig. 2*A*). To test whether the difference in collective migration might have been mediated by a soluble secreted factor, induced after GPR97 knockdown, we added conditioned media, which were collected from scrambled control and from GPR97-deficient cells, to control scrambled and GPR97-deficient LECs. The addition of the conditioned medium from GPR97-deficient LECs did not result in any major changes of migration of scrambled control cells, as compared with the addition of conditioned medium from control cells (Fig. 2*B*). Similarly, the addition of the conditioned media did also not change the migration of GPR97-deficient LECs (Fig. 2*B*).

Silencing of GPR97 Leads to a Redistribution of the Actin Cytoskeleton and of the Focal Adhesion Protein Vinculin—Changes in cell motility are often accompanied by cytoskeletal rearrangements. To further investigate the mechanisms by which loss of GPR97 might affect cell migration, the organization of the F-actin-positive cytoskeleton and of the focal adhesion protein vinculin was investigated. Scrambled control LECs displayed a clustered stress fiber-like F-actin architecture (Fig. 3*A*), in contrast to the plasma membrane-subjacent F-actin fibers in GPR97 knockdown LECs (Fig. 3*B*). The intensity of F-actin staining was significantly reduced after GPR97 knockdown (Fig. 3*C*). Knockdown of GPR97 also resulted in significantly more abundant vinculin clusters (Fig. 3*D*). In contrast, we could not observe a significant change in total β-actin as detected by Western blotting and as compared with the loading control MAPK and with another cytoskeletal protein cofilin (see Fig. 7, *A* and *E*).

The Perturbed Balance of Cdc42 and RhoA after GPR97 Knockdown Is Sufficient to Enhance Collective Cell Migration of LECs—Cytoskeletal redistributions often result from alterations in the activation state of the small Rho GTPases. We determined the levels of active Cdc42 and RhoA in scrambled control *versus* GPR97-targeting siRNA-transfected LECs preceding the cytoskeletal changes (approximately 36 h after knockdown) and detected elevated levels of active Cdc42 (2-fold increase as compared with control; Fig. 4*B*) and decreased levels of active RhoA (from 3.4% of total RhoA in the control to 2.6% in the GPR97-silenced LECs; Fig. 4*C*) after GPR97 knockdown. As a positive control, the known activators of Cdc42 and RhoA, CN02 and CN03, respectively, were applied to the cells prior to lysis. Cdc42 activation resulted in a slight increase (1.3-fold as compared with unstimulated state)

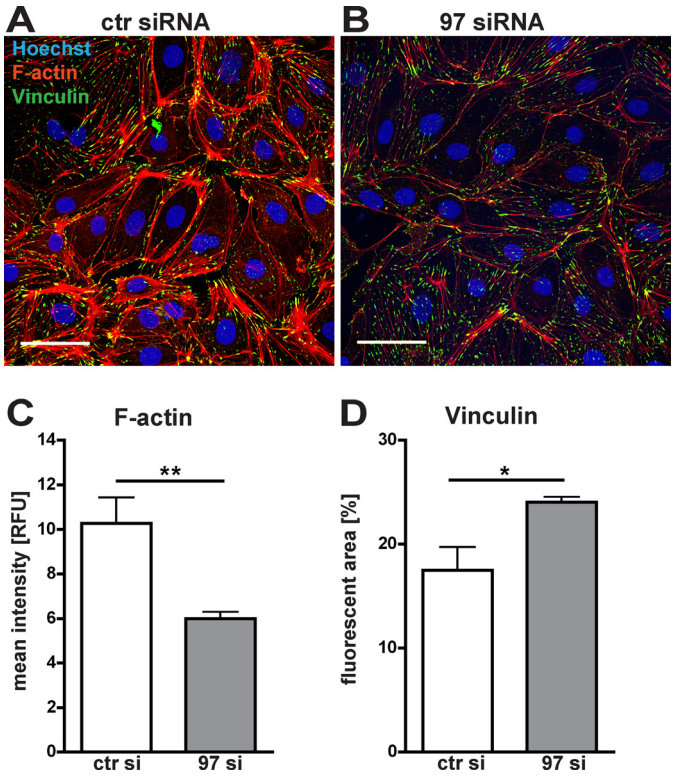

FIGURE 3. **Distribution of F-actin and the focal adhesion protein vinculin after GPR97 knockdown was altered.** *A*, fluorescent staining of F-actin (*red*, rhodamine-phalloidin staining), vinculin (*green*, immunostaining), and cell nuclei (*blue*, Hoechst 33342) in control *versus* GPR97 knockdown LECs; confocal images are shown. *Scale bar* = 50 μm. *ctr siRNA*, control siRNA. *B* and *C*, mean fluorescent intensity (F-actin) (*B*) and fluorescence covered area (vinculin) were determined with ImageJ (*C*). *97 siRNA*, GPR97-targeting siRNA; *RFU*, relative fluorescence units. Mean ± S.E. of $n = 4$ images per condition is shown. *, $p < 0.05$, **, $p < 0.01$.

of GTP-bound Cdc42 in the control LECs. In contrast, the high levels of active Cdc42 in the GPR97-deficient LECs were already saturated because no further activation by CN02 was observed (Fig. 4*A*). Total Cdc42 was slightly increased (1.3-fold, Fig. 4, *D* and *E*) but not to levels that could account for the dramatic difference in activated Cdc42. CN03 increased the active fraction of RhoA from 3.4 to 4.9% in control LECs (1.5-fold) but more strongly activated RhoA (1.8-fold from 2.6 to 4.7%) in GPR97-deficient LECs. The RhoA-GTP levels in the CN03-treated GPR97-deficient LECs were comparable with those of the unstimulated control LECs, indicating that RhoA in the GPR97-deficient cells is functional. We next investigated whether the observed alterations in the balance between active Cdc42 and RhoA might be crucial for the effects of GPR97 knockdown on cell migration. Control and GPR97-deficient LECs were incubated with the Cdc42 activator CN02 or the RhoA activator CN03 from $t = 0$ h until $t = 4$ h in the wound healing assay. Activation of Cdc42 by CN02 significantly enhanced wound closure of control LECs, to a similar extent as GPR97 knockdown (Fig. 4*F*). *Vice versa*, activation of RhoA by CN03 reversed the increased cell migration after GPR97 knockdown to control levels (Fig. 4*G*).

GPR97-deficient Cells Display Decreased Single Cell Migration and Increased Adhesion—Because wound closure in the two-dimensional monolayer scratch assay includes aspects of collective migration and/or adhesion, we next investigated the effect of GPR97 loss in Boyden chamber assays on single cell migration (without a gradient of the coating substrate or the chemoattractant), haptotaxis (creating a haptotactic stimulus with fibronectin on the bottom side of the membrane), and chemotaxis (the addition of 3% FBS to the lower chamber). Surprisingly, single cell migration of GPR97-deficient LECs was significantly decreased in comparison with the scrambled control LECs (Fig. 5*A*). However, no major differences were found when chemotactic migration (Fig. 5*B*) and haptotactic migration (Fig. 5*C*) were analyzed. The opposing effects of GPR97 loss in wound healing *versus* Transwell migration suggested that cell adhesion effects might have been involved. Thus, we next determined the adhesion of GPR97-deficient *versus* control LECs to fibronectin and type I collagen. Indeed, LECs transfected with GPR97-targeting siRNA displayed significantly increased adhesion to both fibronectin and type I collagen, as compared with the scrambled control LECs (Fig. 5*D*).

Increased Activation of β1-Integrin in GPR97-deficient LECs—Because adhesion to both fibronectin and collagen I was enhanced in the GPR97-deficient LECs, we analyzed the activation state of the β1-integrin subunit known to be part of both the fibronectin and the type I collagen receptor. To determine the extent of β1-integrin activation, we used the monoclonal antibody 9EG7 that was reported to bind exclusively to the active conformation of β1-integrin (27). We stained single cell suspensions of GPR97-deficient and scrambled control LECs in the presence of Mg^{2+} and detected the active β1-integrin by flow cytometry. In three independent experiments, we found an increase in the mean fluorescent intensity of active β1-integrin in the GPR97-deficient LECs as compared with the control LECs in the same experiment (Fig. 6, *A* and *C*). In addition, confocal microscopy analysis of stained cell cultures also revealed an increased activation of the β1-integrin after GPR97 knockdown (Fig. 6, *D* and *E*). No change in total β1-integrin was detected (Fig. 6*B*). Quantification of the integrated fluorescence area of activated β1-integrin normalized to total β1-integrin reveals a significantly higher value for the GPR97-deficient LECs (Fig. 6*F*).

Increased Phosphorylation of PAK4 and Paxillin in GPR97-deficient LECs—Because the canonical G protein-mediated GPCR signaling involves different kinases and the observed cytoskeletal changes often result from phosphorylation of cytoskeletal proteins, we sought to elucidate the link between GPR97 and the cytoskeleton. We found no phosphorylation changes of protein kinase B (AKT) and protein kinase C (PKC) (Fig. 7*D*), Src (Fig. 7*C*), or MAPK (Fig. 7*D*) representing the major downstream kinases of GPCR signaling. No alteration could be detected in the phosphorylation state of MLC and cofilin (Fig. 7, *B* and *C*), two cytoskeletal proteins involved in cellular motility. However, phosphorylation of PAK4, a downstream target of Cdc42, and paxillin was slightly higher in the GPR97-deficient cells (Fig. 7, *A* and *F* and *C* and *G*, respectively).

DISCUSSION

Based on the important role of lymphatic vessel activation in many different diseases, including cancer progression, chronic inflammation, and organ transplant rejection (28), there is a

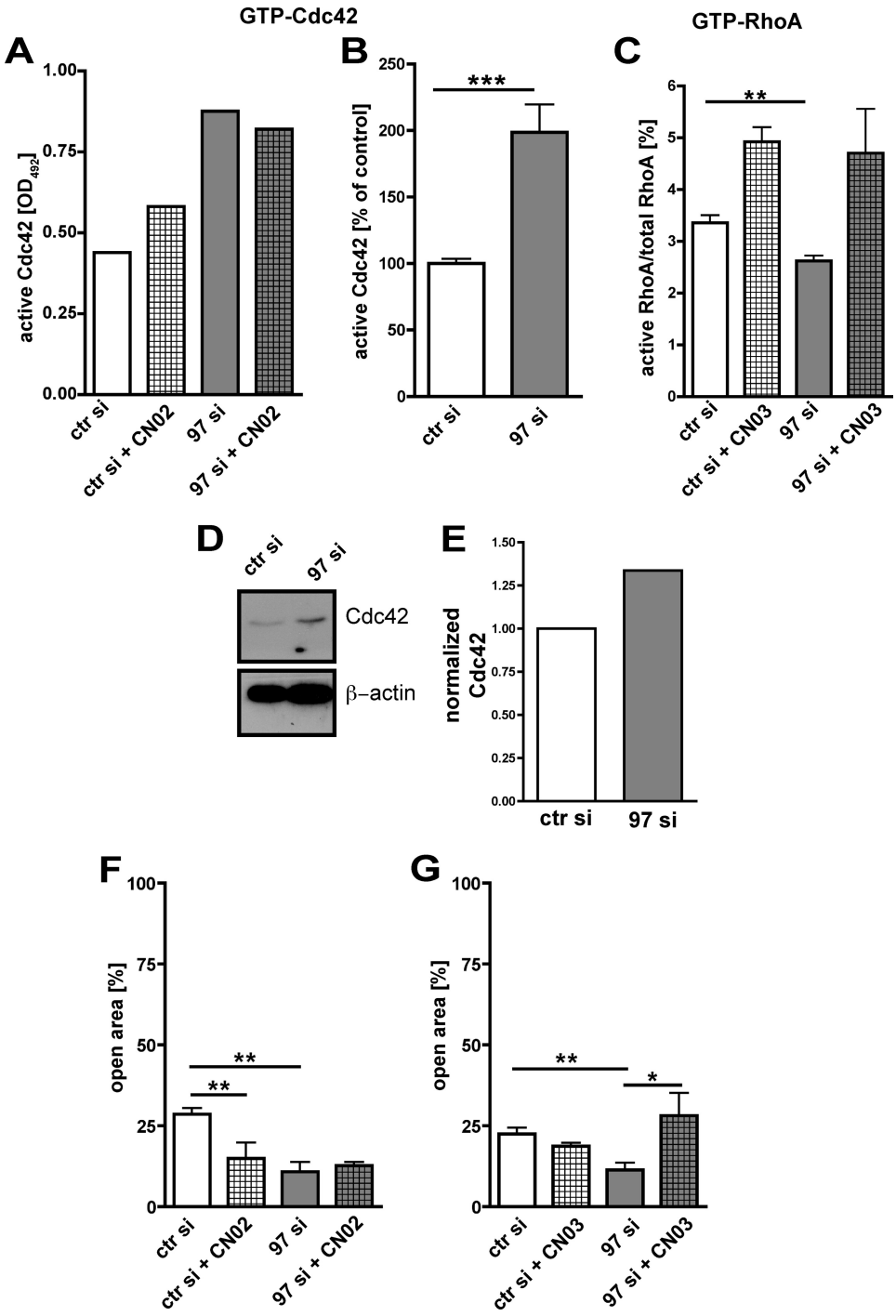

FIGURE 4. **The enhanced migration of GPR97-deficient LECs is linked to perturbations in the levels of activated RhoA and Cdc42.** *A–C*, elevated levels of Cdc42 (*A* and *B*) and decreased levels of active RhoA (*C*) were determined in lysates from GPR97-deficient LECs as compared with scrambled control. The active form of the small GTPases was detected colorimetrically in cell lysates from scrambled control siRNA (*ctr si*) and GPR97-targeting siRNA (*97 si*)-transfected LECs with G-LISA (Cytoskeleton). Cells treated for 2 min with 2 units/ml Cdc42 activator (CN02, Cytoskeleton) and for 30 min with 1 unit/ml RhoA activator (CN03, Cytoskeleton) were used as positive controls for activated Cdc42 and RhoA, respectively. The average optical density at 492 (OD_{492}) of duplicates measured in one experiment is shown in *A*, and the average across three experiments is shown in *B* and *C*. *B*, active Cdc42 was normalized to the scrambled control and averaged from three experiments. *C*, GTP-RhoA was normalized to total RhoA as determined by ELISA (Cytoskeleton), and the average percentage of active RhoA across three experiments is presented. *D* and *E*, total Cdc42 was determined by Western blotting (*D*), and the bands were densitometrically quantified with ImageJ and normalized to the loading control β-actin (*E*). *F* and *G*, activation of RhoA reversed (*F*) and activation of Cdc42 phenocopied (*G*) the migratory phenotype of GPR97-deficient cells in monolayer wound healing assay. Quantification of the wounded area (in %) of control *versus* GPR97-deficient LECs that remained open at $t = 17$ h was performed by TScratch software tool. Treatment with 0.5 unit/ml RhoA activator CN03 could reverse the enhanced migration of GPR97-deficient LECs to control levels, and treatment with 1 unit/ml Cdc42 activator CN02 could enhance migration of control siRNA-transfected LECs to the levels of the GPR97-deficient cells. Mean ± S.E., $n = 4$ wells per condition (average of two scratches per well) is shown. *, $p < 0.05$, **, $p < 0.01$, ***, $p < 0.001$.

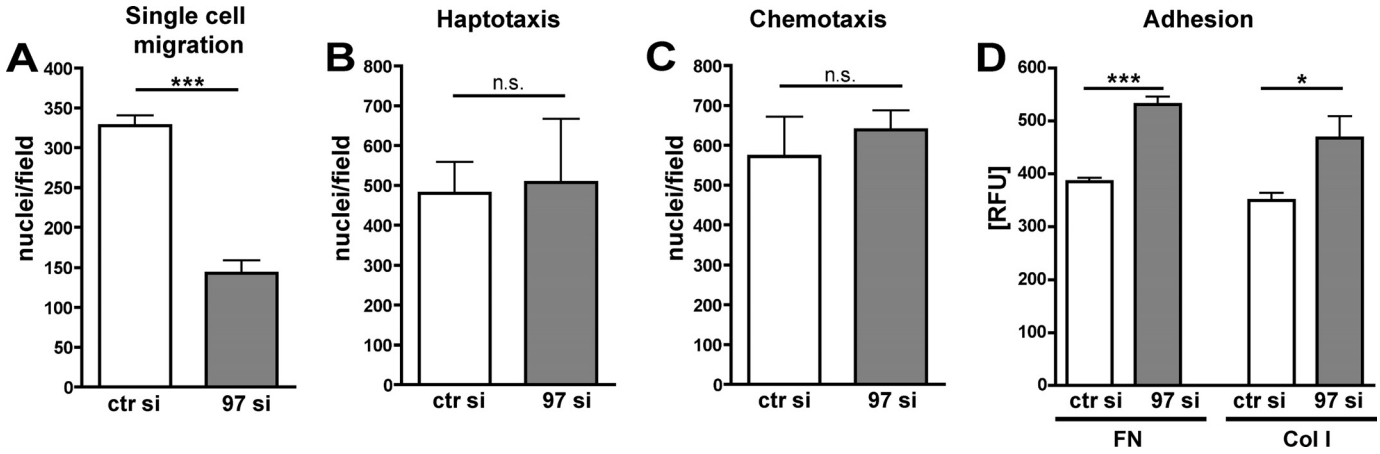

FIGURE 5. **GPR97 knockdown decreases single cell motility in the absence of chemo- and haptoattractants and increases adhesion.** *A–C*, GPR97-deficient LECs showed decreased single cell motility (*A*) but no significant difference in the haptotactic (*B*) and chemotactic (*C*) behavior as compared with control siRNA-transfected cells. Transwell migration assay through 8-μm pores was utilized for the analysis of single cell migration (both sides of the membrane coated with 10 μg/ml fibronectin), chemotaxis (3% FBS in the lower chamber), and haptotaxis (coating of the bottom cell-free side of the membrane with 10 μg/ml fibronectin). 4 h after seeding, the transmigrated cells were fixed and stained with Hoechst 33342. The number of nuclei per visual field (average of five fields per membrane) was determined with ImageJ. Bars represent mean ± S.E. of triplicates per condition. ***, $p < 0.001$. ctr si, control siRNA; *97 si*, GPR97-targeting siRNA. *D*, increased adhesive properties of LECs transfected with GPR97-targeting siRNA (*97 si*) *versus* control siRNA. LECs were detached 40 h after transfection, incubated in suspension with 4 μg/ml calcein-AM in PBS for 15 min, and seeded on 96-well plates coated with fibronectin (*FN*, 10 μg/ml) or type I collagen (*Col I*, 50 μg/ml). The floating cells were discarded after 45 min with three washing steps, and the fluorescence ($\lambda_{ex} = 485$ nm, $\lambda_{em} = 530$ nm) of the adherent cells was used as a measure for the cell number. *RFU*, relative fluorescence units. Mean ± S.E., $n = 8$ wells is shown. *, $p < 0.05$, ***, $p < 0.001$.

need to identify suitable molecular targets for the specific pharmacological manipulation of lymphangiogenesis. Because the GPCRs are a highly druggable protein family, we sought to identify GPCRs that are specifically expressed by the lymphatic endothelium as compared with the blood vascular endothelium. Indeed, using an *ex vivo* protocol to specifically isolate LECs and BECs from the mouse intestine, we identified a range of GPCRs that are exclusively or more strongly expressed by LECs, including Gprc5c, Gpr77, Gpr124, and Celsr1. In addition, we found that the adrenomedullin receptor is more strongly expressed by LECs, in agreement with recent studies (29).

Because GPR97 was the GPCR with the most specific expression in LECs, and because little is known about the potential function of this adhesion-type GPCR, we focused our studies on the characterization of the potential biological role of this receptor. GPR97 is a member of the large class of adhesion GPCRs that are characterized by their unique combination of cell adhesion and signaling properties (17). GPR97 was first isolated from a cDNA library derived from mouse pre-B cells and thymocytes, and the only published study on the potential function of GPR97 has focused on its role in early lymphoid development (30). However, loss of GPR97 did not affect *in vivo* B and T cell maturation, suggesting a functional redundancy with another protein (30).

In the present study, we found that GPR97 is also expressed in cultured human LECs, at both the RNA and the protein level. Transient knockdown studies in these cells indicated that GPR97 moderates collective cell migration and cell adhesion, but that it enhances single cell migration. A similar dichotomous effect on the migratory behavior of endothelial cells has been reported for another protein abundantly expressed by endothelial cells: PECAM-1, for which a role in balancing the different types of endothelial cell movement has been suggested (31). The GPR97-mediated effects might be more relevant for quiescent endothelium because the induction of migration by chemotactic and haptotactic stimuli overcame the reduced motility of GPR97-deficient LECs, possibly due to compensatory mechanisms downstream of other receptors. For instance, the chemokine receptors represent another GPCR group that also regulates directed cell migration (32). In line with our results, the highly homologous adhesion GPCR GPR56 has been reported to inhibit cell migration of neural progenitor cells (26, 33) and cancer cell metastasis (25). Recently, GPR56 was also implicated in angiogenesis during cancer progression (34) through a mechanism involving increased VEGF-A secretion by melanoma cells. In contrast, our results indicate that GPR97 directly regulates cell migration without an intermediary soluble factor because conditioned medium from GPR97-deficient cells did not increase migration of LECs.

Our data provide the first evidence that GPR97 regulates cellular motility by potentially interfering with the mechanisms that maintain the equilibrium between the small G proteins RhoA and Cdc42 leading to F-actin redistribution and focal adhesion rearrangements. The role of these small GTPases in cell migration in wound healing and in single cell migration has been described in detail by Nobes and Hall (35). In line with our findings, Cdc42 activation in rat embryonic fibroblasts was found to be required for collective cell migration, whereas active Cdc42 attenuated single cell motility. Additionally, active RhoA antagonized Cdc42 in both processes. Cdc42 activation and RhoA inhibition have also been implicated in the angiogenic activation of microvascular endothelial cells by VEGF-A (36). Similar to our observations, augmented Cdc42 activity induced the redistribution of F-actin stress fibers to cortical F-actin. Our observation that VEGF-A did not significantly increase the migration of GPR97-deficient LECs supports the idea that VEGF-A stimulation and GPR97 knockdown might affect similar pathways. Although RhoA and Cdc42 might be concurrently regulated downstream of GPR97, a direct inter-

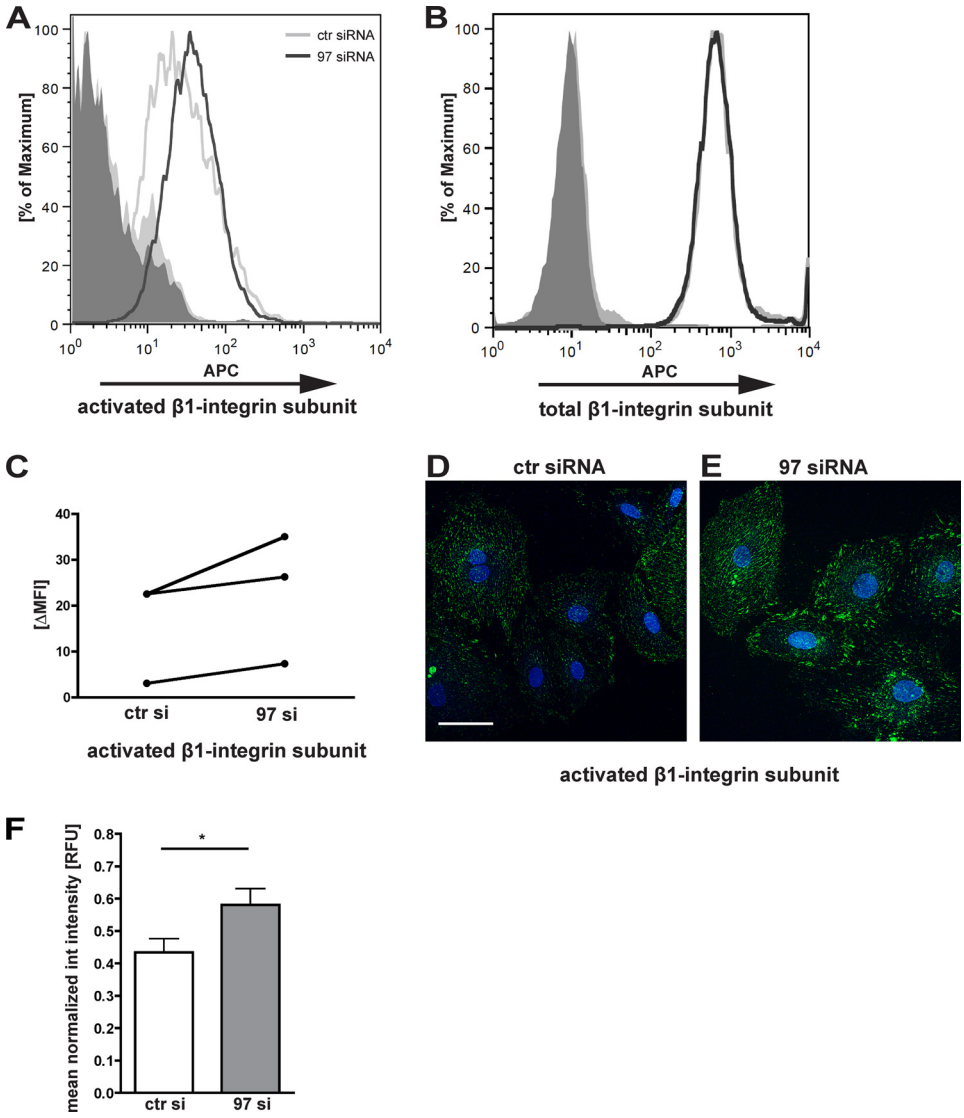

FIGURE 6. **GPR97-deficient LECs show enriched active β1-integrin subunit.** Specific detection of activated β1 integrin was facilitated by the monoclonal 9EG7 antibody reported to recognize only the active conformation of the antigen. *A* and *B*, single cell suspensions of GPR97-targeting siRNA (*97 siRNA*) *versus* control siRNA (*ctr siRNA*) LECs stained for either activated β1 integrin (*A*, *open histograms*) or total β1 integrin (*B*, *open histograms*) and the corresponding isotype controls IgGs (*A* and *B*, *shaded histograms*) were visualized in flow cytometry with allophycocyanin (*APC*)-labeled goat antibody. *C*, the activation state in scrambled control and GPR97-deficient LECs of three independent experiments is represented as mean fluorescent intensity (MFI) of activated β1 integrin after subtraction of the mean fluorescent intensity of the corresponding IgG control (indicated as Δ*MFI*). The pairs of each experiment are connected with a *line*. *D* and *E*, immunofluorescent staining of active β1 integrin (*green*) in scrambled control (*D*) or GPR97-targeting siRNA (*E*)-transfected LECs. Representative confocal images are shown; *scale bar* = 50 μm. *F*, mean fluorescent integrated intensity (activated β1 integrin normalized to overall β1 integrin) was determined with ImageJ. *RFU*, relative fluorescence units. Mean $\pm$ S.E. of $n = 12$ images per condition is shown. *, $p < 0.05$.

play between RhoA and Cdc42 is also possible. Active RhoA can inhibit Cdc42 and the establishment of cell polarity (37) and, *vice versa*, active Cdc42 can directly suppress basal RhoA activity (36).

Our data suggest that the increased adhesive properties of GPR97-deficient LEC might be mediated, at least in part, by increased activation of the β1-integrin subunit and possibly reinforced by enhanced formation of nascent focal adhesions as suggested by the abundant vinculin expression. There are several possible mediators between the small GTPases and the integrin in the GPR97-deficient cells. For instance, abolished RhoA activation in epithelial cells leads to stabilization of the focal adhesion kinase (FAK)-$\alpha 2\beta 1$ integrin complex and to increased cell attachment and spreading (38). The increased adhesion might be mediated by direct binding of active β1-integrin to its extracellular matrix substrates type I collagen and fibronectin, in line with our finding that increased adhesion and migration of GPR97-deficient cells were observed on both substrates.

Regarding the signaling molecules that link GPR97 to the small GTPases and the observed cytoskeletal rearrangements, there are still many open questions. In the GPR97-deficient cells, we observed an increased phosphorylation of the cytoskeletal adapter molecule paxillin at Tyr-31. This is in line with the increased recruitment of vinculin and activated β1-integrin and would suggest an enhanced formation of focal adhesions and increased migration potential. However, Src phosphorylation reported to be a downstream event of β1-integrin activa-

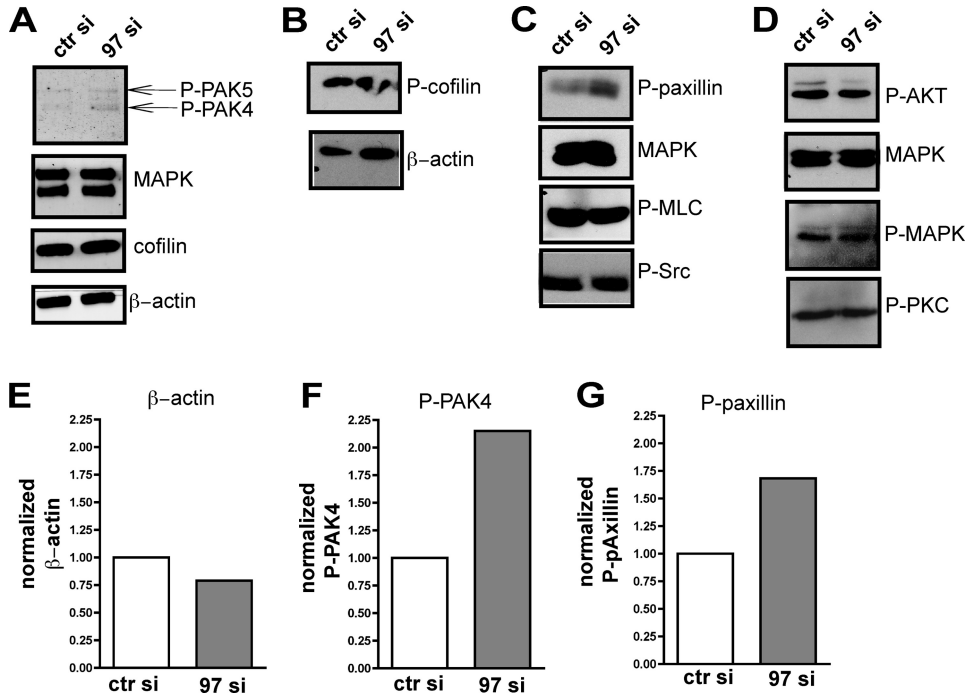

FIGURE 7. **GPR97-deficient LECs show slightly increased phosphorylation of PAK4 (Ser-474) and paxillin (Tyr-31).** *A–D*, the representative phosphorylation state of PAK4, PAK5, and PAK6 (*A*), cofilin (*B*), paxillin, MLC, and Src (*C*) and AKT, MAPK, and PKC (*D*) from three independent experiments is shown as detected by Western blotting using phospho-specific antibodies. MAPK and β-actin served as loading controls. *ctr si*, control siRNA; *97 si*, GPR97-targeting siRNA. Differences in p-PAK4 and p-paxillin were quantified densitometrically with ImageJ and normalized to the loading control MAPK (*F* and *G*, respectively). β-Actin levels were compared with another cytoskeletal protein cofilin (*A*), densitometrically quantified (ImageJ), and normalized to MAPK (*E*).

tion was not altered. Furthermore, phosphorylation of PAK4 reported to be a target of Cdc42 and PKC crucial for endothelial lumen formation was mildly elevated (39). To find a link between G protein-mediated signaling and the cytoskeletal rearrangements, we screened the phosphorylation state of PKC and AKT as downstream kinases of $G\alpha_q$ and $G\beta\gamma$ and MAPK, MLC, and cofilin as downstream targets of $G\alpha_{12/13}$ (mediated by the small GTPases). None of the potential targets were differentially phosphorylated in the GPR97-deficient LECs as compared with the scrambled control. Nevertheless, their involvement in the mentioned pathways in GPR97-governed processes cannot be completely excluded because the cytoskeletal effects might not be linked to classical G protein-coupled signaling after receptor activation. The major obstacle to distinguish between these two possibilities remains the lack of known ligand(s). Only very recently, a comprehensive study has been conducted in a heterologous CHO/HEK 293 overexpression system to systematically screen a library of compounds for agonists of the orphan adhesion GPCRs (18). Notably, this study provided the first information in this regard, indicating that beclomethasone induces GPR97-dependent $G\alpha_{qo3}$ signaling. However, we did not observe a modulation of collective cell migration upon treatment of LECs with beclomethasone (data not shown). This discrepancy may be due to differences in the downstream cellular response after stimulation of the overexpressed receptor in CHO/HEK293 cells and of the endogenous receptor in LECs. Additionally, the two readouts, a direct second messenger measurement and a complex cellular response, cannot be compared directly. Gupte *et al.* (18) and other recent studies (reviewed in Ref. 40) conclude that surprisingly, the vast majority of adhesion GPCRs are capable of signaling through the canonical GPCR downstream mediators: the heterotrimeric G proteins. In the context of GPR97-regulated cell migration and adhesion, several $G\alpha$ subunit isoforms as well as the $G\beta\gamma$ dimer of the heterotrimeric complex could be involved (21). In terms of protein binding properties, GPCR signaling through $G\alpha_{q/11}$ often binds also to $G\alpha_{12/13}$. The well characterized downstream signaling of the latter involves activation of RhoA (41). A recent study shows that inhibition of vascular smooth muscle cell migration is governed by the sphingosine 1-phosphate receptor 2 ($S1P_2$) receptor and is mediated by both $G\alpha_{12/13}$ and $G\alpha_q$ (42). Moreover, analogy to GPR56-mediated inhibition of migration through $G\alpha_{12/13}$ and $G\alpha_q$ favors this hypothesis (33, 43).

Importantly however, our data cannot exclude another mechanism of action of GPR97; because the adhesion GPCRs also exhibit noncanonical, purely adhesive modes of action (40), it is possible that GPR97 interacts directly or at least in a G protein-independent manner with the β1 integrin subunit and/or the focal adhesion protein vinculin and hampers β1 integrin activation. In this scenario, increased activation of β1 integrin upon loss of GPR97 triggers the observed cellular rearrangements because activated β1 integrin can also activate Cdc42 (44). This would be an alternative explanation for the fact that beclomethasone, as an activator of G protein-mediated downstream signaling, did not affect *in vitro* wound healing (data not shown).

Taken together, our study provides the first insights into the cellular function of the poorly characterized adhesion GPCR GPR97, which we have found to be specifically expressed by lymphatic endothelium but not by blood vascular endothelium. It will be of great interest to investigate, in future studies,

whether GPR97 might also play a role in the development and function of the lymphatic vascular system or in lymphangiogenesis under pathological conditions. Given the cell type-restricted expression pattern of adhesion GPCRs and the recent advances in the field (40, 45), the identification of GPR97 as a lymphatic adhesion GPCR might open new possibilities for the future pharmacological manipulation of lymphangiogenesis.

Acknowledgments—We thank Dr. Klaus Seuwen and Dr. Marie-Gabrielle Ludwig for helpful discussions.

REFERENCES

1. Cueni, L. N., and Detmar, M. (2008) The lymphatic system in health and disease. *Lymphat. Res. Biol.* **6,** 109–122
2. Tammela, T., and Alitalo, K. (2010) Lymphangiogenesis: Molecular mechanisms and future promise. *Cell* **140,** 460–476
3. Alitalo, K. (2011) The lymphatic vasculature in disease. *Nat. Med.* **17,** 1371–1380
4. Christiansen, A., and Detmar, M. (2011) Lymphangiogenesis and cancer. *Genes Cancer* **2,** 1146–1158
5. Huggenberger, R., Siddiqui, S. S., Brander, D., Ullmann, S., Zimmermann, K., Antsiferova, M., Werner, S., Alitalo, K., and Detmar, M. (2011) An important role of lymphatic vessel activation in limiting acute inflammation. *Blood* **117,** 4667–4678
6. Huggenberger, R., Ullmann, S., Proulx, S. T., Pytowski, B., Alitalo, K., and Detmar, M. (2010) Stimulation of lymphangiogenesis via VEGFR-3 inhibits chronic skin inflammation. *J. Exp. Med.* **207,** 2255–2269
7. Alitalo, A., and Detmar, M. (2012) Interaction of tumor cells and lymphatic vessels in cancer progression. *Oncogene* **31,** 4499–4508
8. Jacoby, E., Bouhelal, R., Gerspacher, M., and Seuwen, K. (2006) The 7 TM G-protein-coupled receptor target family. *Chem. Med. Chem.* **1,** 761–782
9. Dunworth, W. P., and Caron, K. M. (2009) G protein-coupled receptors as potential drug targets for lymphangiogenesis and lymphatic vascular diseases. *Arterioscler. Thromb. Vasc. Biol.* **29,** 650–656
10. Kriehuber, E., Breiteneder-Geleff, S., Groeger, M., Soleiman, A., Schoppmann, S. F., Stingl, G., Kerjaschki, D., and Maurer, D. (2001) Isolation and characterization of dermal lymphatic and blood endothelial cells reveal stable and functionally specialized cell lineages. *J. Exp. Med.* **194,** 797–808
11. Hirakawa, S., Hong, Y. K., Harvey, N., Schacht, V., Matsuda, K., Libermann, T., and Detmar, M. (2003) Identification of vascular lineage-specific genes by transcriptional profiling of isolated blood vascular and lymphatic endothelial cells. *Am. J. Pathol.* **162,** 575–586
12. Petrova, T. V., Mäkinen, T., Mäkelä, T. P., Saarela, J., Virtanen, I., Ferrell, R. E., Finegold, D. N., Kerjaschki, D., Ylä-Herttuala, S., and Alitalo, K. (2002) Lymphatic endothelial reprogramming of vascular endothelial cells by the Prox-1 homeobox transcription factor. *EMBO J.* **21,** 4593–4599
13. Jurisic, G., Maby-El Hajjami, H., Karaman, S., Ochsenbein, A. M., Alitalo, A., Siddiqui, S. S., Ochoa Pereira, C., Petrova, T. V., and Detmar, M. (2012) An unexpected role of semaphorin3a-neuropilin-1 signaling in lymphatic vessel maturation and valve formation. *Circ. Res.* **111,** 426–436
14. Jurisic, G., Iolyeva, M., Proulx, S. T., Halin, C., and Detmar, M. (2010) Thymus cell antigen 1 (Thy1, CD90) is expressed by lymphatic vessels and mediates cell adhesion to lymphatic endothelium. *Exp. Cell Res.* **316,** 2982–2992
15. Fredriksson, R., Lagerström, M. C., Höglund, P. J., and Schiöth, H. B. (2002) Novel human G protein-coupled receptors with long N-terminals containing GPS domains and Ser/Thr-rich regions. *FEBS Lett.* **531,** 407–414
16. Yona, S., Lin, H.-H., Siu, W. O., Gordon, S., and Stacey, M. (2008) Adhesion-GPCRs: emerging roles for novel receptors. *Trends Biochem. Sci.* **33,** 491–500
17. Bjarnadóttir, T. K., Fredriksson, R., and Schiöth, H. B. (2007) The adhesion GPCRs: a unique family of G protein-coupled receptors with important roles in both central and peripheral tissues. *Cell. Mol. Life Sci.* **64,** 2104–2119
18. Gupte, J., Swaminath, G., Danao, J., Tian, H., Li, Y., and Wu, X. (2012) Signaling property study of adhesion G-protein-coupled receptors. *FEBS Lett.* **586,** 1214–1219
19. Mizuno, N., and Itoh, H. (2010) Signal transduction mediated through adhesion-GPCRs. *Adv. Exp. Med. Biol.* **706,** 157–166
20. Yona, S., Lin, H. H., and Stacey, M. (2010) Immunity and adhesion-GPCRs. *Adv. Exp. Med. Biol.* **706,** 121–127
21. Cotton, M., and Claing, A. (2009) G protein-coupled receptors stimulation and the control of cell migration. *Cell Signal* **21,** 1045–1053
22. Adams, R. H., and Alitalo, K. (2007) Molecular regulation of angiogenesis and lymphangiogenesis. *Nat. Rev. Mol. Cell Biol.* **8,** 464–478
23. Livak, K. J., and Schmittgen, T. D. (2001) Analysis of relative gene expression data using real-time quantitative PCR and the $2^{-\Delta\Delta CT}$ method. *Methods* **25,** 402–408
24. Gebäck, T., Schulz, M. M., Koumoutsakos, P., and Detmar, M. (2009) TScratch: a novel and simple software tool for automated analysis of monolayer wound healing assays. *BioTechniques* **46,** 265–274
25. Xu, L., Begum, S., Hearn, J. D., and Hynes, R. O. (2006) GPR56, an atypical G protein-coupled receptor, binds tissue transglutaminase, TG2, and inhibits melanoma tumor growth and metastasis. *Proc. Natl. Acad. Sci. U.S.A.* **103,** 9023–9028
26. Luo, R., Jeong, S. J., Jin, Z., Strokes, N., Li, S., and Piao, X. (2011) G protein-coupled receptor 56 and collagen III, a receptor-ligand pair, regulates cortical development and lamination. *Proc. Natl. Acad. Sci. U.S.A.* **108,** 12925–12930
27. Lenter, M., Uhlig, H., Hamann, A., Jenö, P., Imhof, B., and Vestweber, D. (1993) A monoclonal antibody against an activation epitope on mouse integrin chain β1 blocks adhesion of lymphocytes to the endothelial integrin $\alpha_6\beta_1$. *Proc. Natl. Acad. Sci. U.S.A.* **90,** 9051–9055
28. Jurisic, G., and Detmar, M. (2009) Lymphatic endothelium in health and disease. *Cell Tissue Res.* **335,** 97–108
29. Fritz-Six, K. L., Dunworth, W. P., Li, M., and Caron, K. M. (2008) Adrenomedullin signaling is necessary for murine lymphatic vascular development. *J. Clin. Invest.* **118,** 40–50
30. Sleckman, B. P., Khan, W. N., Xu, W., Bassing, C. H., Malynn, B. A., Copeland, N. G., Bardon, C. G., Breit, T. M., Davidson, L., Oltz, E. M., Jenkins, N. A., Berman, J. E., and Alt, F. W. (2000) Cloning and functional characterization of the early-lymphocyte-specific Pb99 gene. *Mol. Cell. Biol.* **20,** 4405–4410
31. Gratzinger, D., Canosa, S., Engelhardt, B., and Madri, J. A. (2003) Platelet endothelial cell adhesion molecule-1 modulates endothelial cell motility through the small G-protein Rho. *FASEB J.* **17,** 1458–1469
32. Scholten, D. J., Canals, M., Maussang, D., Roumen, L., Smit, M. J., Wijtmans, M., de Graaf, C., Vischer, H. F., and Leurs, R. (2012) Pharmacological modulation of chemokine receptor function. *Br. J. Pharmacol.* **165,** 1617–1643
33. Iguchi, T., Sakata, K., Yoshizaki, K., Tago, K., Mizuno, N., and Itoh, H. (2008) Orphan G protein-coupled receptor GPR56 regulates neural progenitor cell migration via a $G\alpha_{12/13}$ and Rho pathway. *J. Biol. Chem.* **283,** 14469–14478
34. Yang, L., Chen, G., Mohanty, S., Scott, G., Fazal, F., Rahman, A., Begum, S., Hynes, R. O., and Xu, L. (2011) GPR56 Regulates VEGF production and angiogenesis during melanoma progression. *Cancer Res.* **71,** 5558–5568
35. Nobes, C. D., and Hall, A. (1999) Rho GTPases control polarity, protrusion, and adhesion during cell movement. *J. Cell Biol.* **144,** 1235–1244
36. Ispanovic, E., Serio, D., and Haas, T. L. (2008) Cdc42 and RhoA have opposing roles in regulating membrane type 1-matrix metalloproteinase localization and matrix metalloproteinase-2 activation. *Am. J. Physiol. Cell Physiol.* **295,** C600–C610
37. Shum, M. S., Pasquier, E., Po'uha, S. T., O'Neill, G. M., Chaponnier, C., Gunning, P. W., and Kavallaris, M. (2011) γ-Actin regulates cell migration and modulates the ROCK signaling pathway. *FASEB J.* **25,** 4423–4433
38. Kong, T., Xu, D., Yu, W., Takakura, A., Boucher, I., Tran, M., Kreidberg, J. A., Shah, J., Zhou, J., and Denker, B. M. (2009) $G\alpha_{12}$ inhibits $\alpha2\beta1$ integrin-mediated Madin-Darby canine kidney cell attachment and migration on collagen-I and blocks tubulogenesis. *Mol. Biol. Cell* **20,** 4596–4610
39. Koh, W., Sachidanandam, K., Stratman, A. N., Sacharidou, A., Mayo,

A. M., Murphy, E. A., Cheresh, D. A., and Davis, G. E. (2009) Formation of endothelial lumens requires a coordinated PKCϵ-, Src-, Pak- and Raf-kinase-dependent signaling cascade downstream of Cdc42 activation. *J. Cell Sci.* **122,** 1812–1822

40. Paavola, K. J., and Hall, R. A. (2012) Adhesion G protein-coupled receptors: signaling, pharmacology, and mechanisms of activation. *Mol. Pharmacol.* **82,** 777–783
41. Buhl, A. M., Johnson, N. L., Dhanasekaran, N., and Johnson, G. L. (1995) $G\alpha_{12}$ and $G\alpha_{13}$ stimulate Rho-dependent stress fiber formation and focal adhesion assembly. *J. Biol. Chem.* **270,** 24631–24634
42. Takashima, S., Sugimoto, N., Takuwa, N., Okamoto, Y., Yoshioka, K., Takamura, M., Takata, S., Kaneko, S., and Takuwa, Y. (2008) G12/13 and Gq mediate $S1P_2$-induced inhibition of Rac and migration in vascular smooth muscle in a manner dependent on Rho but not Rho kinase. *Cardiovasc. Res.* **79,** 689–697
43. Little, K. D., Hemler, M. E., and Stipp, C. S. (2004) Dynamic regulation of a GPCR-tetraspanin-G protein complex on intact cells: central role of CD81 in facilitating GPR56-$G\alpha_{q/11}$ association. *Mol. Biol. Cell* **15,** 2375–2387
44. King, S. J., Worth, D. C., Scales, T. M., Monypenny, J., Jones, G. E., and Parsons, M. (2011) β1 integrins regulate fibroblast chemotaxis through control of N-WASP stability. *EMBO J.* **30,** 1705–1718
45. Araç, D., Boucard, A. A., Bolliger, M. F., Nguyen, J., Soltis, S. M., Südhof, T. C., and Brunger, A. T. (2012) A novel evolutionarily conserved domain of cell-adhesion GPCRs mediates autoproteolysis. *EMBO J.* **31,** 1364-1378